Research papers

State of health estimation of lithium-ion batteries using Autoencoders and Ensemble Learning

Ji Wu [a], Junxiong Chen [a], Xiong Feng [a], Haitao Xiang [b], Qiao Zhu [a],*

[a] *School of Mechanical Engineering, Southwest Jiaotong University, Chengdu, 610031, China*
[b] *College of Mining Engineering, Taiyuan University of Technology, Taiyuan, 030024, China*

ABSTRACT

This paper focuses on the state of health (SOH) estimation of lithium-ion batteries, which is critical for the reliable operation of electric vehicles. First, a convolutional autoencoder (AE) and a recurrent AE are designed to automatically extract health features (HFs), which are the low-dimensional mappings of the charging profiles at different aging stages. This feature extraction method with two AEs can avoid the artificial definition of HFs and the additional operation on the charging profiles. On this basis, an ensemble learning (EL) method is proposed to improve the SOH estimation accuracy, which consists of a series of sequentially trained gate recurrent unit (GRU) networks. This pattern of sequential training makes that the current GRU network can focus on the poor-performing samples of the previous trained network. Finally, four battery datasets under different cycling test conditions are used to verify the efficiency of the proposed SOH estimation method with the two AEs and the EL. The experimental results reveal that the proposed method can provide accurate battery SOH estimation, with the root mean square error and mean absolute error of Leave-One-Out cross validation (LOO) are 1.04% and 0.77%.

1. Introduction

With the goal of peak carbon dioxide emissions and carbon neutrality proposed in various countries, electric vehicles have attracted more and more attention. Lithium-ion batteries have become the preferred choice for electric vehicle power battery because of their high energy density, long lifespan and high working voltage [1]. However, with the increase of the running time of the battery, its performance will inevitably decline, resulting in aging phenomena such as the decrease of capacity and the increase of internal resistance [2]. Hence, the accurate estimation of state of health (SOH) to reflect the aging status of the battery is crucial to the rational use and replacement of the battery. In addition, accurate state of charge (SOC) relies on the correction of the maximum available capacity of the battery by the SOH, thus ensuring safe and reliable operation of electric vehicles [3].

1.1. Literature review

At present, there are a variety of relevant estimation approaches have been proposed, which can be roughly divided into three categories: empirical model-based methods, battery model-based methods, and machine learning (ML)-based methods. Empirical model-based methods are to obtain the battery life decay model by fitting the

laboratory aging data. A set of models representing battery aging characteristics in different cycles and calendars were established by using interactive multiple model Kalman filter, and the most representative model was selected [4]. Considering the interaction between battery aging and electrothermal behavior, Ecker et al. [5] coupled the impedance-based electrothermal model to the original aging model. However, the accuracy of the empirical models are limited to the conditions similar to the experimental data, so they are difficult to apply to the real vehicle operation.

Battery model-based methods generally establish the battery model at first, and then employ adaptive algorithms to identify the battery aging parameters, and finally calculate the SOH. Common battery models include the equivalent circuit model (ECM) and the electrochemical model (EM). In Ref. [6], the parameters such as resistance and capacitance which can reflect aging in the second-order ECM was estimated by genetic algorithm (GA) in real time. Considering the influence of aging parameters on the estimation accuracy of SOC, Song et al. [7] adopted multi-scale extended Kalman filter to update SOC and the first-order ECM parameters. However, accurate estimation of battery model parameters depends on accurate SOC, which is directly related to the available capacity of the battery and is generally difficult to obtain. EMs are a class of models that can describe the internal reactions

and characteristics of battery, such as Pseudo-Two-Dimensional (P2D) model and single particle model (SPM) [8]. In Ref. [9], an SPM-based degradation model was developed by including Solid Electrolyte Interface (SEI) layer formation, which can quickly predict capacity fade according to the cycle number and temperature. However, with a series of nonlinear coupled partial differential equations, the high computational difficulty and load of EM hinders its practicability.

ML-based methods get more attention because of their high precision and model independence characteristics [10]. The current ML-based methods for SOH estimation are mainly divided into two steps. First, the health features (HFs) that can reflect the aging degree are extracted from the charging data, and then the mapping relationship between these HFs and SOH is established. The reason for extracting HFs is that the original charging sequence is too long to be directly used as input, otherwise the large number of model parameters will lead to inefficient calculation and easy over-fitting. Common HFs are extracted from the following sources. At most, the geometric or statistical features of the charging curves are selected as the HFs, such as the time stamp when the voltage reaches the interval point [11], the slope of local curve [12], sample entropy of voltage [13], etc. These features directly reflect the differences of charging curves in different aging degree from different angles. Second, the incremental capacity (IC) curve, obtained by the differential of capacity to voltage, has been proved to clearly show the capacity degradation [14]. In Ref. [15,16], the authors took the positions of the equal-voltage spacing and the positions of the peaks on the IC curve as HFs, respectively. Similar to the IC curve, there is also the differential voltage (DV) curve [17]. Third, some researchers also extracted the HFs from the voltage response curve of pulse current [18,19]. In addition, a few researchers input the original charging data directly into the designed model by increasing the sampling interval [20]. After obtaining the HFs, the ML methods are used to learn the nonlinear relationship between them and capacity. Here, common ML methods for SOH estimation include support vector machine (SVM) [21], Gaussian process regression (GPR) [22], and neural network (NN) [23]. Generally, these methods have strong nonlinear mapping ability.

Although the above-mentioned researches have achieved good performance in feature extraction and model design, there are still two critical problems that can be improved. First, most of the existing HFs are extracted manually, which often requires additional manpower consumption, such as the IC curves that need to be smoothed by filtering algorithms [15,16] and the impulse current response curves that require additional operation on the battery [18,19]. Although some HFs have been proved to be highly related to the battery aging process, their adequacy and availability should be considered. For example, the HFs extracted only from the voltage curves ignore the influence of battery temperature on charging performance [24], and the duration of constant current (CC) phase and constant voltage (CV) phase requires complete charging data that is difficult to obtain in the actual operation of the battery [25]. Therefore, a more reliable and convenient HFs extraction method is needed. Considering that battery aging is a time-related process, some researchers have applied gated recurrent neural network (RNN) to the SOH estimation problem, this is a neural network that can utilize past information to improve the accuracy of current estimation [26]. In Ref. [27] and Ref. [28], an long short-term memory (LSTM) network and a gate recurrent unit (GRU) network were used to estimate SOH, respectively. As two extensions of RNN, the GRU and LSTM have similar performance in improving the long-term dependencies of RNN, but the structure of the former is simpler than that of the latter. However, the performance of neural networks is highly data-dependent, and the acquisition of battery aging data is generally time-consuming and laborious. Therefore, to improve the SOH estimation accuracy of the gated RNN under the condition of limited number of samples is the second problem to be addressed in this study. Ensemble learning (EL), a class of methods that integrates

multiple differential learners through a certain strategy to improve accuracy and robustness, is a feasible solution for the proposed problem. Shen et al. [29] trained eight convolution neural networks (CNN) and employed a fully-connected ensemble layer to combine the capacity estimates. In Ref. [30], the random forest was used to capture the relationship between the extracted HFs and SOH. However, in these bagging EL methods, the similar training sets and the independent properties result in the base learners having similar variances and biases, so their ensemble focuses more on reducing the estimation variance rather than bias. In contrast, the boosting algorithms that can effectively reduce the estimation bias should get more attention in the SOH estimation problem. In addition, the base learners used by existing EL methods cannot make full use of previous measurements to predict the current SOH value.

1.2. Motivation and contributions

In order to solve the two problems mentioned above, this paper proposes a combined SOH estimation method based on autoencoders (AEs) and ensemble learning (EL). First, a convolutional AE (CAE) and a recurrent AE (RAE) are designed to automatically extract HFs from the partial charging voltage and temperature curves. Then, based on the extracted HFs, an EL method using the GRU network as the base learner is proposed to estimate the SOH. Finally, the proposed method is validated by the Leave-One-Out cross validation and compared with other existing SOH estimation methods. The main contributions of the paper are elaborated below:

(1) The proposed AEs can automatically extract the low-dimensional maps of the partial charging voltage and temperature profiles as the HFs. Compared with the manual extraction methods, this method avoids artificially defining HFs and does not require additional operations on the charging profiles or the batteries. The experimental results demonstrate that the extracted HFs can be effectively used for SOH estimation.

(2) An EL algorithm is introduced to the GRU network, which first gives weights to the original dataset, and then adjusts the weights according to the results of the trained GRU network to make the new GRU network focus more on the previous samples with poor performance. In this way, the method can use the limited number of samples to obtain a strong learner composed of a set of distinct and associated GRU networks, thus improving the accuracy of SOH estimation.

1.3. Organization of the paper

The structure of this paper is arranged as follows: Section 2 introduces the dataset used in this paper and some processing procedures. Section 3 describes two AEs for HFs extraction, namely CAE and RAE. Section 4 presents the proposed AdaBoost algorithm-based EL method for capacity estimation. Section 5 provides the experimental results and discussion. Finally, the paper is summarized in Section 5.

2. Experimental data

2.1. Experimental data analysis

The experimental data used in this paper was obtained from the National Aeronautics and Space Administration (NASA) battery aging dataset, which records the experimental data of charge and discharge experiments on a series of 18650 batteries.

Table 1 lists the detailed operational profiles of the batteries adopted in this paper. It should be noted that the specific charging process is divided into two stages, charging in a constant current (CC) mode at 1.5 A until the battery voltage reached 4.2 V, and then continued in a constant voltage (CV) mode until the charge current dropped to

Table 1
The four batteries' specific cycle condition.

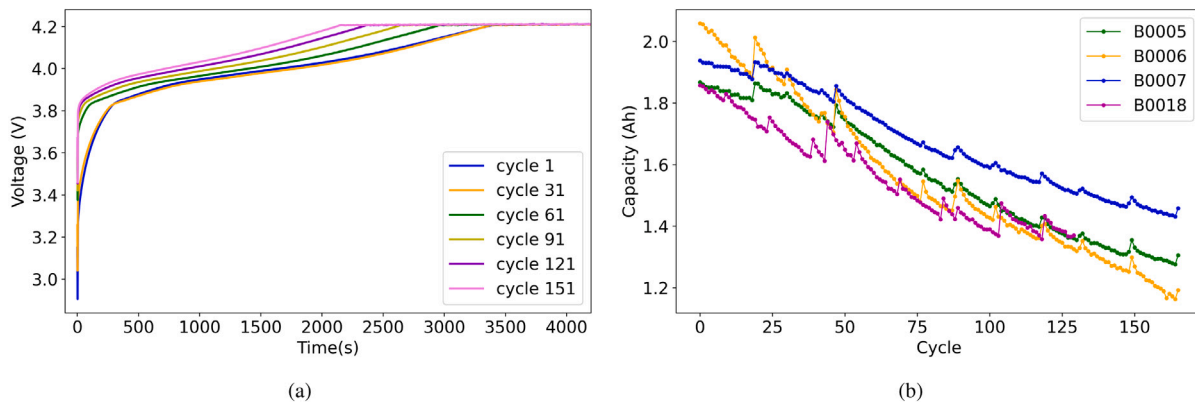| Battery	Charging cut-off voltage (V)	Charging constant current (A)	Discharging cut-off voltage (V)	Discharging constant current (A)	Temperature (°C)
B0005	4.2	1.5	2.7	2	24
B0006	4.2	1.5	2.5	2	24
B0007	4.2	1.5	2.2	2	24
B0018	4.2	1.5	2.5	2	24

Fig. 1. The battery charging profiles and capacity degradation profiles. (a) Charging voltage curves of B0005. (b) Capacity degradation curves of the four batteries.

20 mA. Fig. 1(a) shows the partial charging voltage curves of B0005 under multiple cycles. It can be observed that as the number of cycles increases, the time of the battery charging process in the CC phase is gradually shortened, while the time in the CV phase is gradually increased. In other words, the charging voltage curves are able to reflect the aging process of the battery. Therefore, a large number of researchers have adopted the charging data to estimate SOH [31]. In contrast, the difference and complexity of discharge profiles restrict their scope of application.

In this paper, we also intercepted part of the voltage curve (3.5 V–4.2 V) of each cycle for research, and the difference of the curves in this interval is obvious. Considering that temperature is an important factor affecting charging performance, the charging voltage curves of the same capacity may be different due to different temperatures. Therefore, the temperature curves are also taken as part of the input. The battery capacity is chosen as the prediction target and used to calculate the SOH, the formula is as follows

$$SOH = \frac{C_N}{C_0} \times 100\% \tag{1}$$

where C_N and C_0 are the battery capacities for the current cycle and the initial cycle, respectively. The capacity degradation curves of the selected four batteries are shown in Fig. 1(b). It should be explained that the capacity degradation process does not show a smooth downward trend, which is due to the phenomenon of local capacity regeneration.

2.2. Experimental data processing

After selecting the aging data, the authors processed them as follows. First of all, the sampling intervals of the original charging curves are not uniform. In order to avoid the negative effects on the subsequent model used to process the sequences, the linear interpolation method is applied to distribute the data evenly. Second, the aging experimental data the aging samples have the characteristics of small number and long sequence, which makes the model prone to overfitting in the training process. Therefore, the data augmentation technology is adopted in this paper. Specifically, the long input sequence is sampled at equal intervals into three short sequences and reordered. Since the input and output of the autoencoder are the same, the original
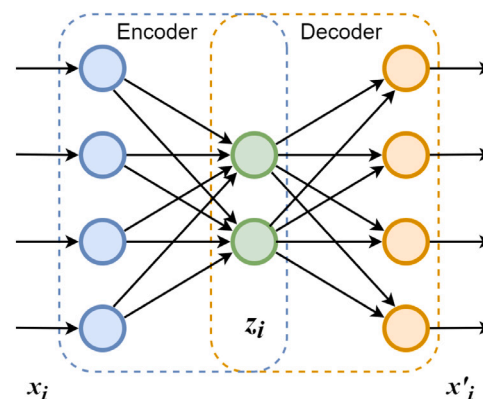

Fig. 2. The structure of a simple autoencoder.

pair of input and output can be expanded into 3×3 groups, which facilitates the autoencoder to extract more representative HFs. Finally, the data is normalized to eliminate the influence of different measurement units and speed up the learning rate of the neural network.

3. Health features extraction

3.1. Autoencoder

As an unsupervised learning neural network, the autoencoder (AE) can automatically learn the effective coding from a set of data, which is often used to reduce data dimensionality or extract features [32]. The AE generally consists of an encoder and a decoder, and its structure is shown in Fig. 2. For a set of D-dimensional samples $x^{(n)} \in R^D, 1 \leq n \leq N$, the encoder F is responsible for mapping them to the feature space to get the coding of each sample $z^{(n)} \in R^M, 1 \leq n \leq N$, as shown in Eq. (1). On the contrary, the decoder G reconstructs the coding from the encoder to the original samples $x'^{(n)}$, as shown in Eq. (2). Therefore, the learning goal of the AE is to minimize the refactoring error τ, as shown in Eq. (3). After completing the training of AE, the decoder is generally removed and the output of the encoder is used as the input of the next step.

Table 2
Specifications of the CAE architecture.

Type	Layer	Input	Kernel number	Step size	Output
Encoder	C	2×512	16	4	16×128
	P	16×128	2	–	16×64
	C	16×64	16	2	16×32
	P	16×32	2	–	16×16
	C	16×16	32	1	32×16
	P	32×16	2	–	32×8
	C	32×8	32	1	32×8
	P	32×8	2	–	32×4
Decoder	TC	32×4	32	2	32×8
	TC	32×8	16	2	16×16
	TC	16×16	16	4	16×64
	TC	16×64	2	8	2×512

C = Convolutional layer, P = Maxpooling layer,
TC = Transposed Convolution layer.

$$z^{(n)} = F(x^{(n)}) \tag{2}$$

$$x'^{(n)} = G(z^{(n)}) \tag{3}$$

$$\tau = \sum_{n=1}^{N} \|x^{(n)} - x'^{(n)}\|^2$$
$$= \sum_{n=1}^{N} \|x^{(n)} - G(F(x^{(n)}))\|^2 \tag{4}$$

Obviously, if the dimension M of the feature space is smaller than that of the original data D, the AE can be regarded as a method of feature extraction. Based on this point, this paper selects AE as the feature extractor to extract effective health features from the charging data, and then use these health features to estimate SOH. It should be pointed out that the hidden layers of simple AE are all fully connected layers. Considering that the charging data are time-based series and compared with ordinary fully connected neural networks, one-dimensional CNN and RNN are adept at dealing with such sequence data. Therefore, we separately designed a convolutional autoencoder (CAE) and a recurrent autoencoder (RAE) to extract health features.

3.2. Structure of the CAE network

Convolution neural network (CNN) is a deep neural network with the characteristics of local connection and weight sharing. Compared with fully connected neural networks, CNN can efficiently find features in large-scale data with fewer parameters, so it is widely used in image processing [33]. Similarly, the characteristics of CNN make it particularly effective for sequence processing, where time can be seen as a spatial dimension. For one-dimensional convolution operation, each output y_i of the convolution kernel w is defined as

$$y_i = f(w \otimes x_i + b)$$
$$= f(\sum_{k=1}^{K} w_k x_{i,k} + b) \tag{5}$$

where x_i is the segment of length K in the input sequence x and K is the length of the convolution kernel, $f(\cdot)$ is the non-linear activation function, such as the ReLU function, $\otimes$ represents the convolution operation, b is the bias. Generally, K is much smaller than the length of the sequence x, so the feature sequence y with definite length can be obtained after selecting the appropriate step size. In fact, we can design multiple convolution kernels to extract different features of the sequence. In addition, a pooling layer is added generally after the convolutional layer to reduce the feature dimension, so as to extract prominent features.
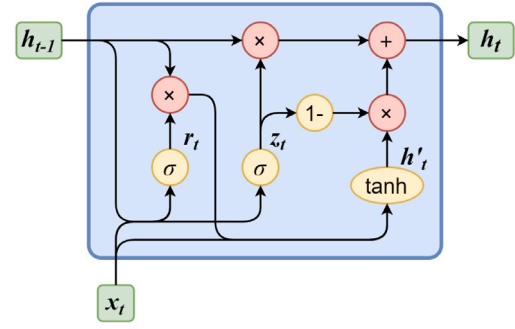

Fig. 3. The architecture detail of GRU cell.

The proposed CAE replaces the original fully connected layers of AE with one-dimensional convolution layers. For the convolution layer, the main parameters include the length and number of convolution kernels, step size and number of layers. Generally, the small convolution kernel not only has a relatively small amount of computation, but also has excellent performance, so smaller kernels and step size are designed in the CAE. With the increase of the convolutional layer, the number of convolution kernels can be appropriately increased to extract higher-level features. In addition, considering the scarcity of samples, too many feature parameters will lead to the over-fitting phenomenon of the SOH estimation in the next step. Therefore, we appropriately increase the number of convolutional layers and add pooling layers to reduce the output dimension of the encoder. Correspondingly, the decoder applies transposed convolution layers to perform the opposite operation to the encoder. The detailed configurations of the designed CAE architecture are shown in Table 2, and its encoder outputs 32 4-dimensional features.

3.3. Structure of the RAE network

Recurrent neural network (RNN) is a kind of neural network with short-term memory ability, which is widely used in tasks such as speech recognition and language modeling [34]. Compared with ordinary fully connected neural network, its current output depends not only on the current input, but also on past information, so it is adept at solving time-related sequences. Furthermore, as a variant of RNN, gated recurrent unit (GRU) network introduces gating mechanism to update information, which solves the problem of gradient disappearance or explosion in ordinary RNN [28]. As shown in Fig. 3, for a GRU unit, it includes an update gate and a reset gate. The reset gate can control whether the calculation of the candidate state h'_t depends on the state of the previous moment h_{t-1}, that is

$$h'_t = \tanh(W_h x_t + U_h(r_t \odot h_{t-1}) + b_h) \tag{6}$$

where x_t is the input of the current moment, $r_t \in [0,1]^D$ is the reset gate, W_h, U_h and b_h are the weight and bias matrices in the neural network, respectively. $\odot$ stands for vector element product operation, $\tanh$ function can push the values to be between -1 and 1. The update gate can control the amount of information that the current state h_t needs to obtain from the historical state h_{t-1} and the candidate state h'_t respectively, that is

$$h_t = z_t \odot h_{t-1} + (1 - z_t) \odot h'_t \tag{7}$$

where $z_t \epsilon [0,1]^D$ is the update gate. The reset gate and the update gate are generated as follows

$$r_t = \sigma(W_r x_t + U_r h_{t-1} + b_r) \tag{8}$$

$$z_t = \sigma(W_z x_t + U_z h_{t-1} + b_z) \tag{9}$$

Table 3
Specifications of the RAE architecture.

Type	Layer	Input	Units	Step size	Output
Encoder	Rs	2×512	–	8	$64 \times 2 \times 8$
	G	$64 \times 2 \times 8$	64	8	$64 \times 64 \times 8$
	G	$64 \times 64 \times 8$	2	1	64×2
Decoder	Rp	64×2	–	8	$64 \times 2 \times 8$
	G	$64 \times 2 \times 8$	64	8	$64 \times 64 \times 8$
	D	$64 \times 64 \times 8$	2	8	$64 \times 2 \times 8$
	Rs	$64 \times 2 \times 8$	–	1	2×512

Rs = Reshape layer, G = GRU layer,
Rp = Repeat layer, D = Dense layer.

where W_r, U_r, W_z, U_z and b_z, b_z are the weight and bias matrices in the reset gate and the update gate. $\sigma(\cdot)$ stands for Logistic function, and its output range is 0 to 1. The structure of the GRU cell is shown in Fig. 3.

Similar to CAE, the proposed RAE replaces the original fully connected layers with GRU layers. However, it is unreasonable to enter the complete charging sequence into the RAE. Although GRU improves the long-term dependence of RNN, its sequential calculation will still cause the long sequence to lose the previous information. In other words, entering the complete charging sequence directly will probably not get the desired results. In addition, too long input sequences will seriously increase the amount of calculation of the GRU layer. Therefore, we split the original sequence into several segments, and the RAE compresses them into several feature vectors. Here, we divide the original charging sequence into 64 segments, and the dimension of each segment is (2, 8). The detailed configurations of the designed RAE are shown in Table 3, and its encoder outputs 64 2-dimensional features.

Remark 3.1. The original charging sequences are too long to be directly used to estimate SOH, which is a challenge for SOH estimation. Therefore, this paper applies the autoencoders to realize the automatic extraction of HFs. Specifically, the designed CAE and RAE extract features with dimensions (32, 4) and (64, 2) from the charging sequence with dimensions $(2, 512 \times 3)$, respectively. The validity of the extracted HFs is judged by the reconstruction error of the sequences, and their value will be evaluated by the final SOH estimation results.

Remark 3.2. Compared with the ordinary autoencoder composed of fully connected layers, both the designed CAE and RAE are not affected by the sequence length. Specifically, the convolution kernels in the CAE are applicable to the entire sequences, and the RAE is applicable to all fragments of the sequences.

4. SOH estimation method

4.1. Ensemble learning

Ensemble learning (EL) is a kind of machine learning method that integrates multiple models through a certain strategy to complete learning tasks. Compared with a single model, EL generally has higher accuracy and stronger robustness [35]. As one of the excellent strategies, the Adaboost algorithm improves the accuracy of the EL by increasing the difference of each weak learner. Specifically, in the process of sequentially training the weak learners, the Adaboost algorithm increases the weights of the samples that are incorrectly predicted by the existing weak learners, so that the next weak learner can *pay more attention* to them. In this paper, the input $x^{(n)}$ and output $y^{(n)}, 1 \leq n \leq N$ are the extracted features and battery capacity respectively, and N is the number of samples. The steps of the algorithm are as follows, where K is the number of weak learners.

(1) Initialize the weights of the training samples

$$\omega_1^{(n)} = \frac{1}{N}, n = 1, 2, \dots, N$$

(2) For $k = 1, 2, \cdots, K$

   a. Use the training set with sample weights $\omega_k^{(n)} = \frac{1}{N}, n = 1, 2, \dots, N$ to train the weak learner $h_k(x)$

   b. Calculate the maximum error of the samples in the training set

$$E_k = \max |y^{(n)} - h_k(x^{(n)})|$$

   c. Calculate the relative error of each sample

$$e_k^{(n)} = \frac{|y^{(n)} - h_k(x^{(n)})|}{E_k}$$

   d. Calculate regression error rate

$$\varepsilon_k = \sum_{n=1}^{N} \omega_k^{(n)} e_k^{(n)}$$

   e. Calculate the weight of the weak learner h_k

$$\alpha_k = \frac{\varepsilon_k}{1 - \varepsilon_k}$$

   f. Update the weights of samples

$$\omega_{k+1}^{(n)} = \frac{\omega_k^{(n)}}{Z_k} \alpha_k^{1 - e_k^{(n)}}$$

   where

$$Z_k = \sum_{n=1}^{N} \omega_k^{(n)} \alpha_k^{1 - e_k^{(n)}}$$

(3) Constitute the strong learner $H(x)$

$$H(x) = \sum_{n=1}^{N} \ln(\frac{1}{\alpha_k}) h'(x)$$

where $h'(x)$ is the median of the weighted outputs $\alpha_k h_k$ of all base learners.

4.2. Structure of the GRU network

The principle of the GRU network has been introduced in Section 3.3, and a GRU network that can accurately estimate the capacity based on the extracted health features is designed here. In this section, a set of hyperparameters was determined by combining the grid search method and empirical tuning. They can be roughly divided into two categories, structural hyperparameters and training hyperparameters. The hidden layers consist of three GRU layers, each with 128 units, and a dropout layer is added after each layer to prevent overfitting. The output layer is a fully-connected (Dense) layer with Sigmoid activation function, and its output range is 0–1. Compared with the structural hyperparameters, the training hyperparameters are easier to be determined. We used the root mean square error (RMSE) as the loss function, which is often adopted in regression problems. For the optimizer, the Adam optimizer can not only calculate efficiently but also adjust the learning rate automatically. More detailed hyperparameters are shown in Table 4.

Remark 4.1. The scarcity of samples will limit the SOH estimation accuracy, which is another challenge for SOH estimation. The proposed EL method can update the weight of HFs according to the SOH estimation results of the previous GRU network, so that the newly trained GRU network can focus on the samples with large errors. Therefore, the accuracy of the global SOH estimation can be improved by assembling multiple GRU networks with their own strengths.

Remark 4.2. Considering that the aging process of the battery is also a time-related problem, so we again apply the GRU network as the base learner for the Adaboost algorithm. In addition, the EL does not require
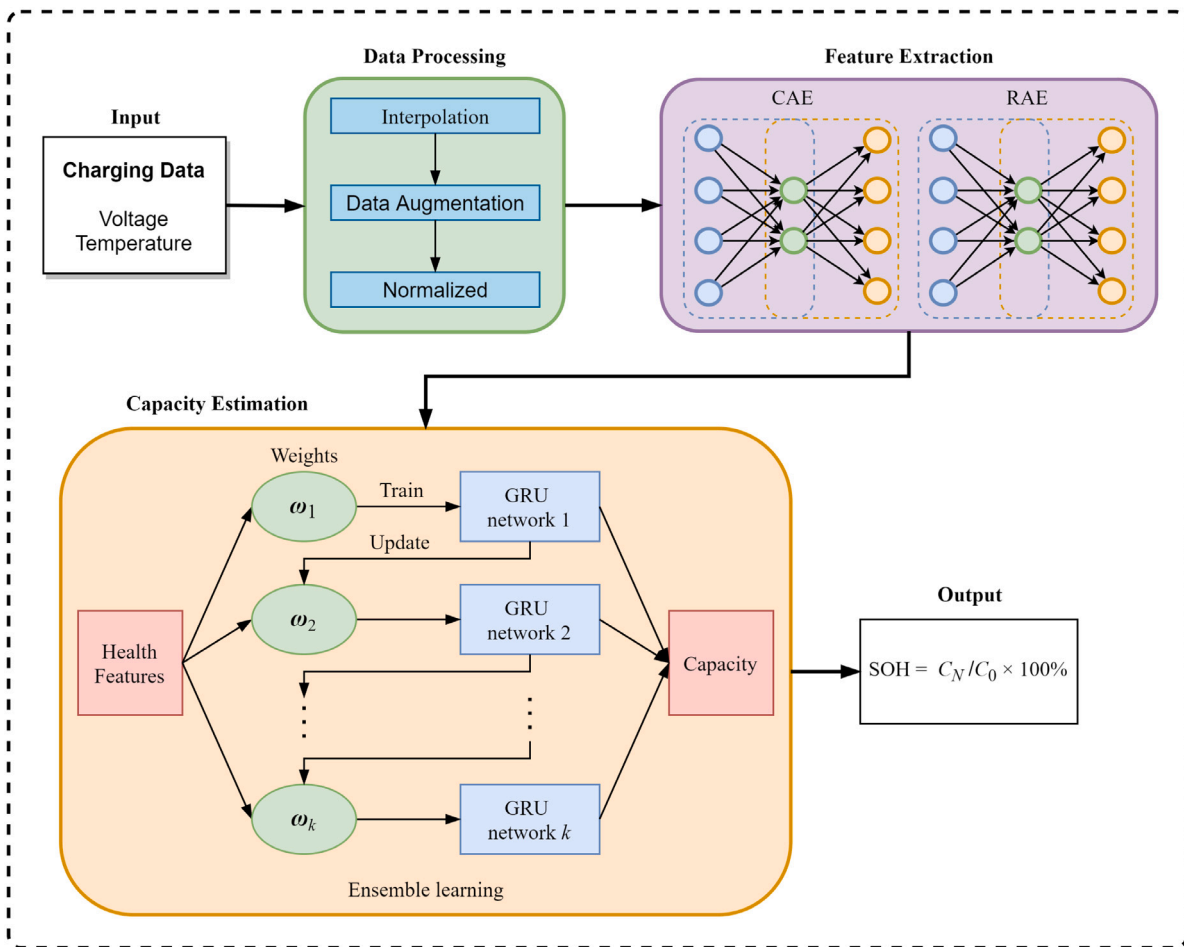
Fig. 4. Framework of the SOH estimation using the proposed combined AEs and EL-GRU method.

Table 4
Hyperparameter settings of the GRU network.

Type	Hyperparameter	Value
Structure	Number of GRU layers	3
	Number of GRU units	128
	Step size	2
	Dropout	0.5
Training	Learning rate	0.001
	Batch size	256
	Training epoch	200
	Optimizer	Adam
	Loss function	RMSE

the optimal hyperparameters of the GRU network, thus reducing the time-consuming and tedious procedure of the SOH estimator design.

4.3. The framework of SOH estimation

The overall framework of the SOH estimation method proposed in this paper is shown in Fig. 4, and the method can be divided into three steps. First, local charging data are selected from the NASA dataset, and processed such as data augmentation and normalization. Then, two autoencoders, CAE and RAE, are designed to automatically extract health features from the charging data. At last, an EL method based on GRU network (EL-GRU) is established to estimate the capacity, and then to obtain the SOH of the lithium battery.

5. Results and discussions

5.1. Network training and evaluation index

In this section, the performance of the proposed combined AEs and the ELGRU method is validated and analyzed using Leave-One-Out cross validation (LOO). Specifically, three of the four batteries are used as the training set and the remaining one as the test set. The proposed combined model is trained and tested four times so that each battery is used to test the model. The result of LOO is the average of the four test results. Meanwhile, the Mean Absolute Error (MAE) and the Root Mean Square Error (RMSE) are adopted to evaluate the performance of the proposed method. They are defined as follows

$$MAE = \frac{1}{N} \sum_{i=1}^{N} |x_i - x'_i| \tag{10}$$

$$RMSE = \sqrt{\frac{1}{N} \left(\sum_{i=1}^{N} \left(x_i - x'_i \right)^2 \right)} \tag{11}$$

where N is the sample size of the test set, and x_i and x'_i are the true and estimated values, respectively.

5.2. Health features extraction with the CAE and RAE

In Section 3, we designed two autoencoders, the CAE and RAE, which can extract 32 four-dimensional features and 64 two-dimensional features respectively. Whether these features are representative and
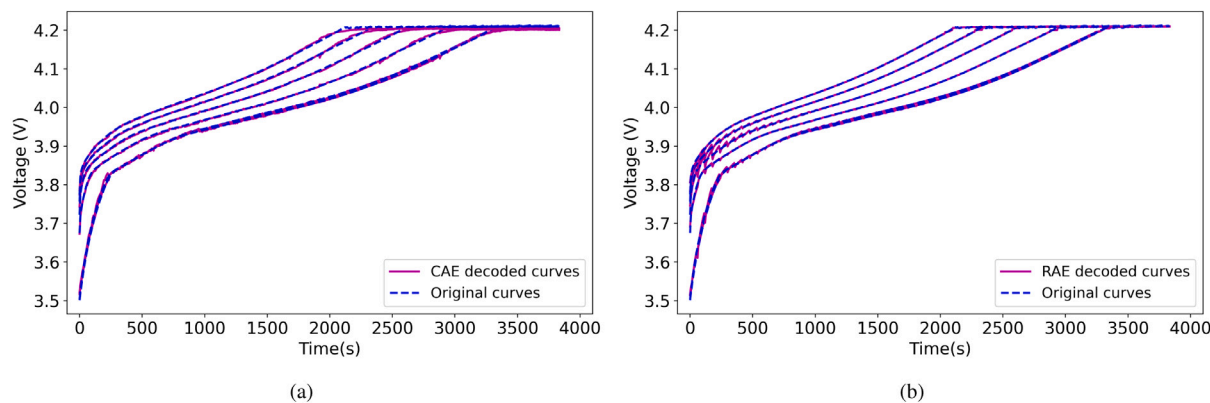
Fig. 5. Decoding results of the CAE and RAE for B0007 at cycles 1, 31, 61, 91, 121, 151. (a) CAE, (b) RAE.

Table 5
Decoding results of the CAE and RAE for four batteries.

Battery		B0005	B0006	B0007	B0018	LOO
CAE	MAE	0.00272	0.00255	0.00345	0.00252	0.00281
	RMSE	0.00369	0.00367	0.00478	0.00533	0.00437
RAE	MAE	0.00103	0.00111	0.00108	0.00114	0.00109
	RMSE	0.00231	0.00323	0.00230	0.00396	0.00295

distinguishable will be verified in this section. The decoding results of the two autoencoders for multiple cycles of the battery B0007 are shown in Fig. 5. Obviously, the decoded temperature and voltage curves can accurately track the original curves, the RMSE is less than 0.005. The detailed decoding errors of all the normalized charging curves are shown in Table 5. The results indicate that the extracted health features can be accurately reduced to charging curves by the corresponding decoders. In other words, these features are able to represent the charging curves.

For the features extracted by the CAE, the number of features is determined by the number of convolution kernels in the last convolution layer, that is, each convolution kernel is a feature extractor. There is no clear correlation between these features, and each feature reflects a local shape of the charging curves. For example, the features extracted by the 5th and 15th convolution kernels are shown in Figs. 6(a) and (b). It can be seen that the trend of the feature vectors extracted from the same convolution kernel is similar, and the differences in specific values are consistent with the aging trend. Different from the CAE, the features extracted by RAE are still time-related sequences. The feature sequences of the two dimensions were compared respectively, as shown in Figs. 6(c) and (d). Obviously, the sharp rise of voltage in the early stage and the voltage inflection point caused by the end of the CC phase are both exhibited. When the voltage is in the CV phase, the difference in the feature curve is caused by the continuous change of temperature. In general, both the CAE and RAE designed in this paper are able to extract distinguishable features from the charging curves of different aging degrees. It should be noted out that whether the SOH can be accurately estimated based on the extracted health features is the main criterion to evaluate the validity of the features. Therefore, we will estimate the SOH of four batteries based on these features in Section 5.3.

5.3. SOH estimation with the EL-GRU network

After the features are extracted by the autoencoders, we will estimate the capacities of four batteries to verify the performance of the proposed combined method in this section. In Section 4, we have designed the GRU network as the base learner of EL. In addition, the

number of base learners was determined to be 10 and the learning rate was 0.2 by comparing multiple groups of parameters in advance. Based on the proposed method, the SOH estimation results and errors of the four batteries are shown in Fig. 7. For the battery B0006, due to its over-discharge operation, the upper and lower limits of capacity far exceeds that of other batteries, as shown in Fig. 1. Therefore, the estimation results of the 30th to 100th cycles (1.43 Ah–1.87 Ah) are intercepted here, as shown in Fig. 7(b). It can be seen that the proposed combination method can accurately track the trend of capacity degradation.

The results show that the proposed combined AEs and the EL-GRU method can accurately estimate the SOH, and the RMSE and MAE of LOO are 1.04% and 0.77%. By observing the SOH prediction results and errors of B0005 and B0007, it is easy to find that large errors often occur in the place of capacity regeneration. The reason is that the base learner of EL, the GRU network, takes the previous results as part of the current input. When the capacity jumps unexpectedly, the continuity of the input sequence disappears, and the network is delayed due to the influence of past information. Nevertheless, the maximum error between the two batteries is still less than 3.2%, and the downward trend of SOH can be tracked after the capacity regeneration. The capacity downward trend of B0006 and B0018 fluctuate more frequently and violently than that of B0005 and B0007, so the errors are relatively larger, with the maximum errors less than 5% and 6%. In addition, the rapid aging of B0006 shows that the study of SOH has important guiding significance for the rational use and life extension of Lithium-ion batteries.

5.4. Comparisons

In order to verify the superiority of the proposed combined method, this section compared it with two other methods, including the GRU network and the EL-GRU network using the manually extracted HFs (labeled as EL-GRU2). The GRU network uses the same HFs as the EL-GRU network. The HFs used by EL-GRU2 network are the timestamps of the equal interval voltages. The comparison of the training results of B0005 is shown in Fig. 8. It can be observed that, compared with the GRU network, the EL-GRU network can re-fit the downward trend of SOH more quickly after capacity recovery occurs. The test results of the three methods for B0005 are shown in Fig. 9, and a detailed comparison of their SOH predictions for the four batteries is shown in Table 6. The results show that the introduction of EL method effectively improves the estimation accuracy of the GRU network, and reduces the RMSE and MAE of LOO from 1.59% and 1.27% to 1.04% and 0.77%. It is also demonstrated that for the SOH estimation, the HFs extracted using the AEs outperform the manually extracted HFs.

Meanwhile, the authors also lists the SOH estimation results of the LSTM network in Table 6. The results show that the GRU and LSTM,
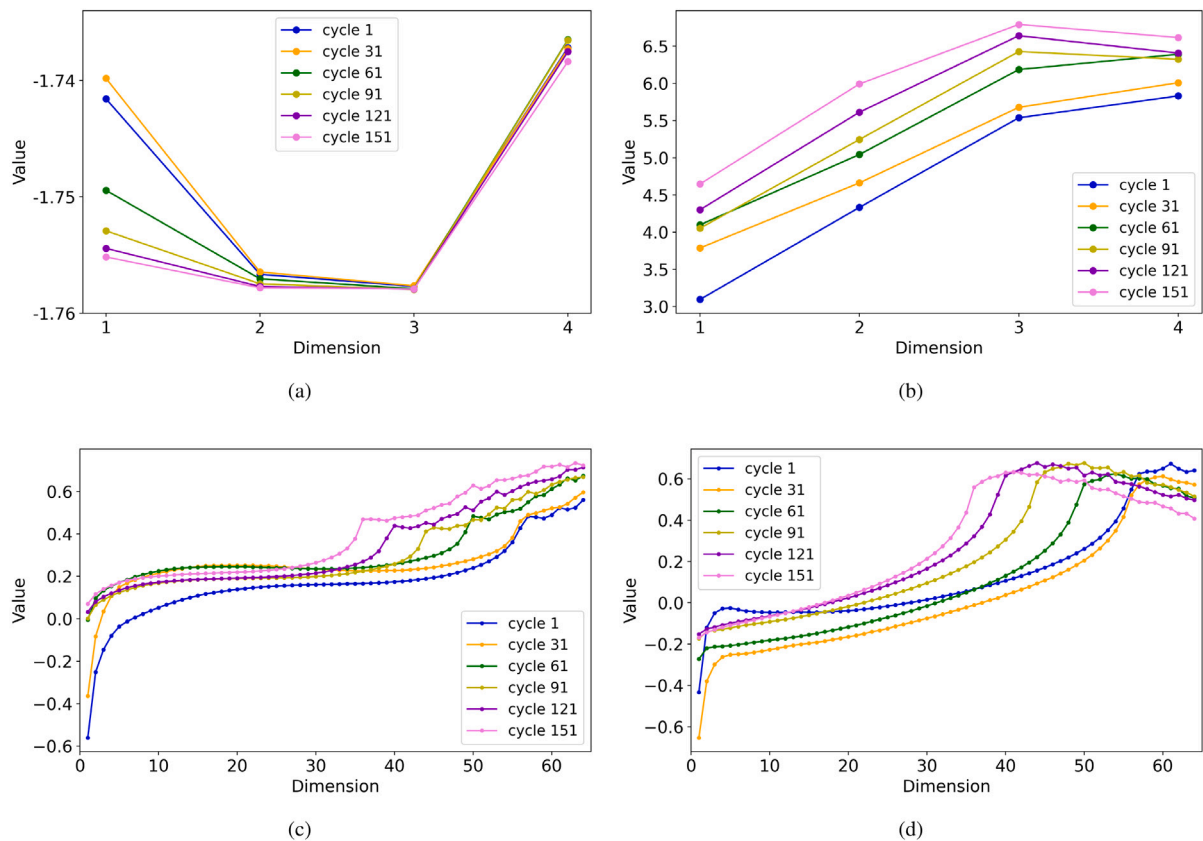
Fig. 6. Health features extracted from B0007 by the CAE and RAE. (a) The 5th feature extracted by CAE. (b) The 15th feature extracted by CAE. (c) The 1st dimension features extracted by RAE. (d) The 2nd dimension features extracted by RAE.

Table 6
Comparison of SOH estimation for four batteries using the proposed method and other methods.

Features source	Model	B0005		B0006		B0007		B0018		LOO	
		MAE	RMSE	MAE	RMSE	MAE	RMSE	MAE	RMSE	MAE	RMSE
CAE + RAE	EL-GRU	0.74%	0.92%	0.70%	1.11%	0.40%	0.59%	1.22%	1.53%	0.77%	1.04%
Charge curves	EL-GRU	2.27%	2.90%	2.45%	2.63%	1.18%	1.47%	1.31%	1.74%	1.80%	2.19%
CAE + RAE	GRU	1.54%	1.73%	1.03%	1.54%	0.57%	0.74%	1.94%	2.35%	1.27%	1.59%
CAE + RAE	LSTM	1.53%	1.80%	1.21%	1.64%	0.68%	0.88%	1.89%	2.47%	1.33%	1.70%
Charge curves	GPR	0.80%	0.96%	1.65%	1.67%	1.21%	1.29%	2.26%	2.28%	1.48%	1.55%
IC curves	SVM	5.21%	1.94%	4.71%	2.16%	4.36%	1.53%	–	–	4.76%	1.88%
IC curves	WNN	1.81%	–	1.61%	–	1.53%	–	1.67%	–	1.66%	–

as two extensions of RNN, have similar accuracy in SOH estimation. Compared with LSTM, the GRU has a simpler structure and fewer parameters, and has higher computational efficiency in theory. However, the decline of battery capacity is slow, and the SOH is generally estimated only once after a long interval, such as a charge–discharge cycle. Therefore, without considering the calculation rate, both the GRU and LSTM can be selected as the base learners of the EL method proposed in this paper. In addition, we also compared the estimation results of the EL-GRU network with the WNN [23], GPR [36], SVM [21] to prove its superiority in estimation accuracy. It should be noted that a large number of literatures use the local aging data of one battery for training and the rest as a test set, while this paper is devoted to predicting the complete aging trend of one battery.

6. Conclusions

A new SOH estimation method has been proposed in this paper by combining two AEs and an EL method. With this method, the health features are first automatically extracted from voltage and temperature charging curves by the CAE and RAE, then the ELGRU is designed to estimate the capacity, and finally the SOH is obtained. To verify the performance of the proposed combined method, four batteries from the NASA dataset are used for training and testing, respectively. Experimental results indicate that the proposed method can accurately estimate the SOH with the RMSE and MAE of LOO are 1.04% and 0.77%. With the proposed method, we neither need to artificially calculate and screen health features, nor need to carefully design the parameters of the GRU network, which are often time-consuming and laborious. Based on the above, this method may have a broad application prospect in practice. Especially with the development of chip and vehicle networking, further hardware support and data support will be provided for the real vehicle application of such data-driven methods.

In future work, the effects of ambient temperature and battery discharge conditions on SOH estimation will be considered. Furthermore, lightweight autoencoders and base learners will be introduced to facilitate the application of the proposed method in real vehicles.
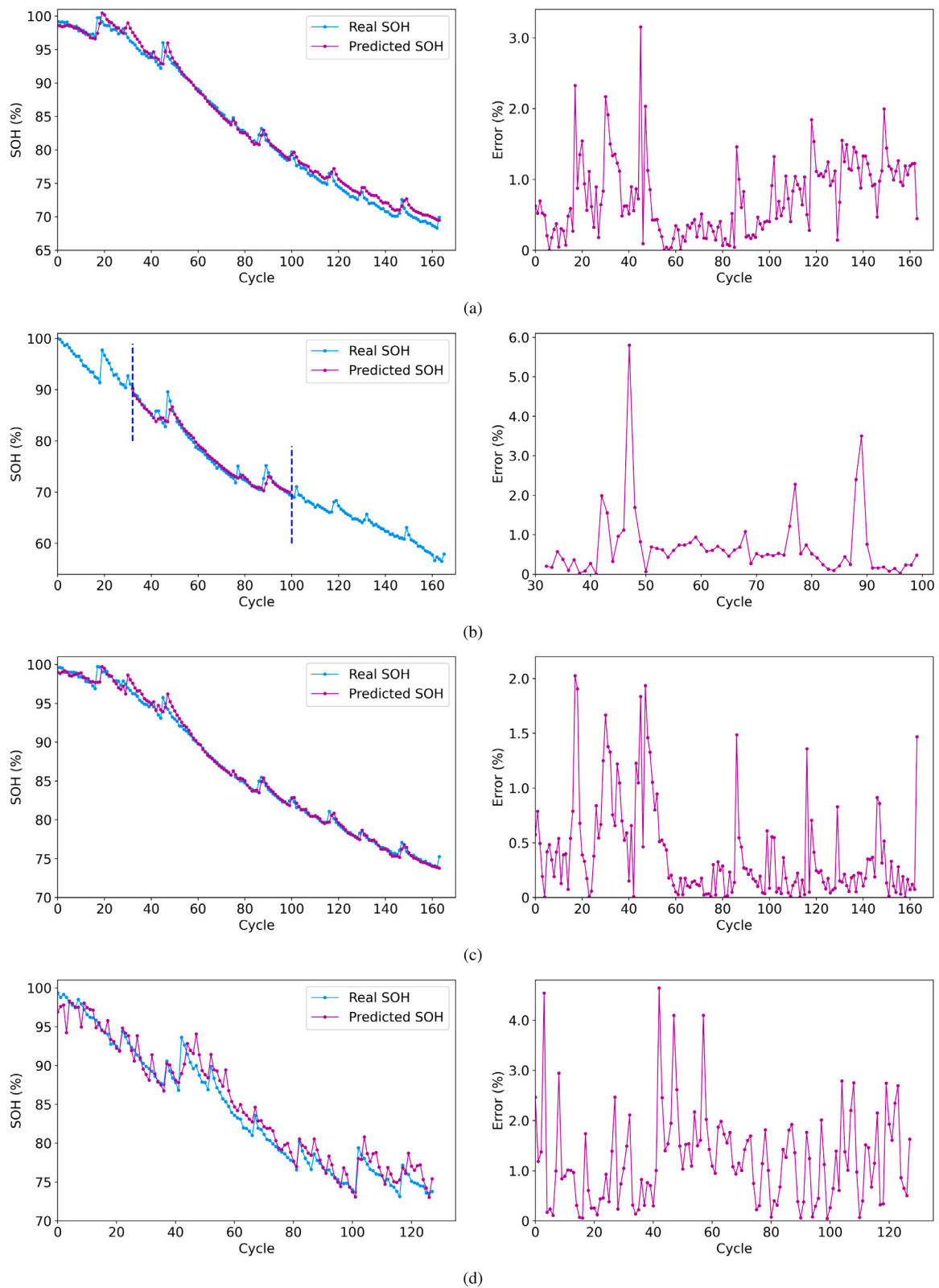
Fig. 7. SOH estimation results of the ELGRU network for four batteries. (a) B0005, (b) B0006, (c) B0007, (d) B0018.
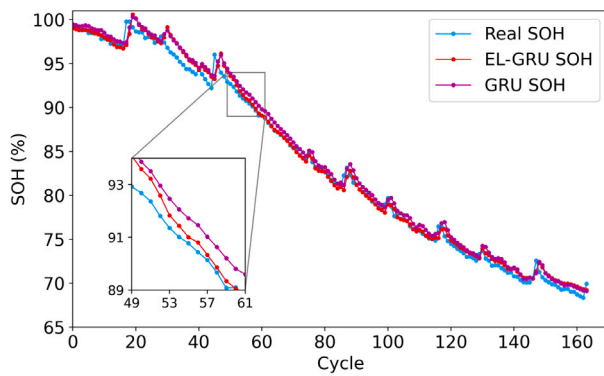
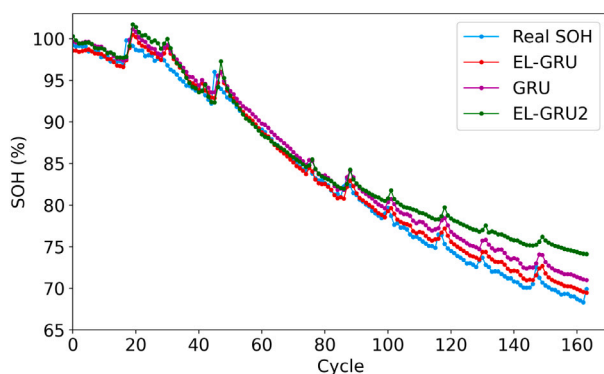**Fig. 8.** Training results of B0005 using the EL-GRU network and the GRU network.

Fig. 9. Text results of B0005 using the three methods, including the EL-GRU, GRU and EL-GRU2.

CRediT authorship contribution statement

Ji Wu: Investigation, Conceptualization, Methodology. **Junxiong Chen:** Software, Validation, Data curation. **Xiong Feng:** Writing – original draft. **Haitao Xiang:** Writing – review & editing. **Qiao Zhu:** Supervision.

Declaration of competing interest

The authors declare that they have no known competing financial interests or personal relationships that could have appeared to influence the work reported in this paper.

Data availability

The authors do not have permission to share data.

References

[1] Y. Wang, J. Tian, Z. Sun, L. Wang, R. Xu, M. Li, Z. Chen, A comprehensive review of battery modeling and state estimation approaches for advanced battery management systems, Renew. Sustain. Energy Rev. 131 (2020) 110015, http://dx.doi.org/10.1016/j.rser.2020.110015, URL https://www.sciencedirect.com/science/article/pii/S1364032120303063.

[2] X. Hu, F. Feng, K. Liu, L. Zhang, J. Xie, B. Liu, State estimation for advanced battery management: Key challenges and future trends, Renew. Sustain. Energy Rev. 114 (2019) 109334, http://dx.doi.org/10.1016/j.rser.2019.109334, URL https://www.sciencedirect.com/science/article/pii/S1364032119305428.

[3] R. Xiong, J. Cao, Q. Yu, H. He, F. Sun, Critical review on the battery state of charge estimation methods for electric vehicles, IEEE Access 6 (2018) 1832–1843, http://dx.doi.org/10.1109/ACCESS.2017.2780258.

[4] A.J. Smiley, W.K. Harrison, G.L. Plett, Postprocessing the outputs of an interacting multiple-model Kalman filter using a Markovian trellis to estimate parameter values of aged li-ion cells, J. Energy Storage 27 (2020) 101043, http://dx.doi.org/10.1016/j.est.2019.101043, URL https://www.sciencedirect.com/science/article/pii/S2352152X19301318.

[5] M. Ecker, J.B. Gerschler, J. Vogel, S. Käbitz, F. Hust, P. Dechent, D.U. Sauer, Development of a lifetime prediction model for lithium-ion batteries based on extended accelerated aging test data, J. Power Sources 215 (2012) 248–257, http://dx.doi.org/10.1016/j.jpowsour.2012.05.012, URL https://www.sciencedirect.com/science/article/pii/S0378775312008671.

[6] Z. Chen, C.C. Mi, Y. Fu, J. Xu, X. Gong, Online battery state of health estimation based on genetic algorithm for electric and hybrid vehicle applications, J. Power Sources 240 (2013) 184–192, http://dx.doi.org/10.1016/j.jpowsour.2013.03.158, URL https://www.sciencedirect.com/science/article/pii/S0378775313005521.

[7] Z. Song, X. Wu, X. Li, J. Sun, H.F. Hofmann, J. Hou, Current profile optimization for combined state of charge and state of health estimation of lithium ion battery based on Cramer–Rao bound analysis, IEEE Trans. Power Electron. 34 (7) (2019) 7067–7078, http://dx.doi.org/10.1109/TPEL.2018.2877294.

[8] R. Xiong, L. Li, J. Tian, Towards a smarter battery management system: A critical review on battery state of health monitoring methods, J. Power Sources 405 (2018) 18–29, http://dx.doi.org/10.1016/j.jpowsour.2018.10.019, URL https://www.sciencedirect.com/science/article/pii/S037877531831111X.

[9] J. Li, K. Adewuyi, N. Lotfi, R. Landers, J. Park, A single particle model with chemical/mechanical degradation physics for lithium ion battery state of health (SOH) estimation, Appl. Energy 212 (2018) 1178–1190, http://dx.doi.org/10.1016/j.apenergy.2018.01.011, URL https://www.sciencedirect.com/science/article/pii/S0306261918300114.

[10] C. Vidal, P. Malysz, P. Kollmeyer, A. Emadi, Machine learning applied to electrified vehicle battery state of charge and state of health estimation: State-of-the-art, IEEE Access 8 (2020) 52796–52814, http://dx.doi.org/10.1109/ACCESS.2020.2980961.

[11] Y. Li, H. Sheng, Y. Cheng, H. Kuang, Lithium-ion battery state of health monitoring based on ensemble learning, in: 2019 IEEE International Instrumentation and Measurement Technology Conference, I2MTC, 2019, pp. 1–6, http://dx.doi.org/10.1109/I2MTC.2019.8826824.

[12] D. Yang, X. Zhang, R. Pan, Y. Wang, Z. Chen, A novel Gaussian process regression model for state-of-health estimation of lithium-ion battery using charging curve, J. Power Sources 384 (2018) 387–395, http://dx.doi.org/10.1016/j.jpowsour.2018.03.015, URL https://www.sciencedirect.com/science/article/pii/S0378775318302398.

[13] X. Sui, S. He, J. Meng, R. Teodorescu, D.-I. Stroe, Fuzzy entropy-based state of health estimation for Li-ion batteries, IEEE J. Emerg. Sel. Top. Power Electron. 9 (4) (2021) 5125–5137, http://dx.doi.org/10.1109/JESTPE.2020.3047004.

[14] X. Li, Z. Wang, L. Zhang, C. Zou, D.D. Dorrell, State-of-health estimation for Li-ion batteries by combing the incremental capacity analysis method with grey relational analysis, J. Power Sources 410–411 (2019) 106–114, http://dx.doi.org/10.1016/j.jpowsour.2018.10.069, URL https://www.sciencedirect.com/science/article/pii/S0378775318311777.

[15] X. Li, Z. Wang, J. Yan, Prognostic health condition for lithium battery using the partial incremental capacity and Gaussian process regression, J. Power Sources 421 (2019) 56–67, http://dx.doi.org/10.1016/j.jpowsour.2019.03.008, URL https://www.sciencedirect.com/science/article/pii/S0378775319302393.

[16] Z. Wang, J. Ma, L. Zhang, State-of-health estimation for lithium-ion batteries based on the multi-island genetic algorithm and the Gaussian process regression, IEEE Access 5 (2017) 21286–21295, http://dx.doi.org/10.1109/ACCESS.2017.2759094.

[17] Z. Wang, C. Yuan, X. Li, Lithium battery state-of-health estimation via differential thermal voltammetry with Gaussian process regression, IEEE Trans. Transp. Electr. PP (2020) http://dx.doi.org/10.1109/TTE.2020.3028784.

[18] J. Meng, L. Cai, D.-I. Stroe, X. Huang, J. Peng, T. Liu, R. Teodorescu, An automatic weak learner formulation for lithium-ion battery state of health estimation, IEEE Trans. Ind. Electron. 69 (3) (2022) 2659–2668, http://dx.doi.org/10.1109/TIE.2021.3065594.

[19] J. Meng, L. Cai, D.-I. Stroe, J. Ma, G. Luo, R. Teodorescu, An optimized ensemble learning framework for lithium-ion battery state of health estimation in energy storage system, Energy 206 (2020) 118140, http://dx.doi.org/10.1016/j.energy.2020.118140, URL https://www.sciencedirect.com/science/article/pii/S0360544220312470.

[20] Y. Fan, F. Xiao, C. Li, G. Yang, X. Tang, A novel deep learning framework for state of health estimation of lithium-ion battery, J. Energy Storage 32 (2020) 101741, http://dx.doi.org/10.1016/j.est.2020.101741, URL https://www.sciencedirect.com/science/article/pii/S2352152X20315784.

[21] J. Tian, R. Xiong, W. Shen, State-of-health estimation based on differential temperature for lithium ion batteries, IEEE Trans. Power Electron. 35 (10) (2020) 10363–10373, http://dx.doi.org/10.1109/TPEL.2020.2978493.

[22] K. Liu, Y. Li, X. Hu, M. Lucu, W.D. Widanage, Gaussian process regression with automatic relevance determination Kernel for calendar aging prediction of lithium-ion batteries, IEEE Trans. Ind. Inf. 16 (6) (2020) 3767–3777, http://dx.doi.org/10.1109/TII.2019.2941747.

[23] C. Chang, Q. Wang, J. Jiang, T. Wu, Lithium-ion b CHANG2021102570 attery state of health estimation using the incremental capacity and wavelet neural networks with genetic algorithm, J. Energy Storage 38 (2021) 102570, http://dx.doi.org/10.1016/j.est.2021.102570, URL https://www.sciencedirect.com/science/article/pii/S2352152X21003157.

[24] W. Li, N. Sengupta, P. Dechent, D. Howey, A. Annaswamy, D.U. Sauer, Online capacity estimation of lithium-ion batteries with deep long short-term memory networks, J. Power Sources 482 (2021) 228863, http://dx.doi.org/10.1016/j.jpowsour.2020.228863, URL https://www.sciencedirect.com/science/article/pii/S0378775320311678.

[25] Y. Wu, Q. Xue, J. Shen, Z. Lei, Z. Chen, Y. Liu, State of health estimation for lithium-ion batteries based on healthy features and long short-term memory, IEEE Access 8 (2020) 28533–28547, http://dx.doi.org/10.1109/ACCESS.2020.2972344.

[26] H. Tian, P. Qin, K. Li, Z. Zhao, A review of the state of health for lithium-ion batteries: Research status and suggestions, J. Cleaner Prod. 261 (2020) 120813, http://dx.doi.org/10.1016/j.jclepro.2020.120813, URL https://www.sciencedirect.com/science/article/pii/S095965262030860X.

[27] Y. Tan, G. Zhao, Transfer learning with long short-term memory network for state-of-health prediction of lithium-ion batteries, IEEE Trans. Ind. Electron. 67 (2019) 8723–8731, http://dx.doi.org/10.1109/TIE.2019.2946551.

[28] M. Jiao, D. Wang, J. Qiu, A GRU-RNN based momentum optimized algorithm for SOC estimation, J. Power Sources 459 (2020) 228051, http://dx.doi.org/10.1016/j.jpowsour.2020.228051, URL https://www.sciencedirect.com/science/article/pii/S0378775320303542.

[29] S. Shen, M. Sadoughi, M. Li, Z. Wang, C. Hu, Deep convolutional neural networks with ensemble learning and transfer learning for capacity estimation of lithium-ion batteries, Appl. Energy 260 (2020) 114296, http://dx.doi.org/10.1016/j.apenergy.2019.114296, URL https://www.sciencedirect.com/science/article/pii/S030626191931983X.

[30] N. Yang, Z. Song, H. Hofmann, J. Sun, Robust state of health estimation of lithium-ion batteries using convolutional neural network and random forest, J. Energy Storage 48 (2022) 103857, http://dx.doi.org/10.1016/j.est.2021.103857, URL https://www.sciencedirect.com/science/article/pii/S2352152X21015231.

[31] Z. Wang, G. Feng, D. Zhen, F. Gu, A. Ball, A review on online state of charge and state of health estimation for lithium-ion batteries in electric vehicles, Energy Rep. 7 (2021) 5141–5161, http://dx.doi.org/10.1016/j.egyr.2021.08.113, URL https://www.sciencedirect.com/science/article/pii/S2352484721007150.

[32] H. Wang, M. jun Peng, Z. Miao, Y. kuo Liu, A. Ayodeji, C. Hao, Remaining useful life prediction techniques for electric valves based on convolution auto encoder and long short term memory, ISA Trans. 108 (2021) 333–342, http://dx.doi.org/10.1016/j.isatra.2020.08.031, URL https://www.sciencedirect.com/science/article/pii/S0019057820303633.

[33] X. Song, F. Yang, D. Wang, K.-L. Tsui, Combined CNN-LSTM network for state-of-charge estimation of lithium-ion batteries, IEEE Access 7 (2019) 88894–88902, http://dx.doi.org/10.1109/ACCESS.2019.2926517.

[34] X. Feng, J. Chen, Z. Zhang, S. Miao, Q. Zhu, State-of-charge estimation of lithium-ion battery based on clockwork recurrent neural network, Energy 236 (2021) 121360, http://dx.doi.org/10.1016/j.energy.2021.121360, URL https://www.sciencedirect.com/science/article/pii/S036054422101608X.

[35] X. Sui, S. He, S.B. Vilsen, J. Meng, R. Teodorescu, D.-I. Stroe, A review of non-probabilistic machine learning-based state of health estimation techniques for lithium-ion battery, Appl. Energy 300 (2021) 117346, http://dx.doi.org/10.1016/j.apenergy.2021.117346, URL https://www.sciencedirect.com/science/article/pii/S0306261921007546.

[36] X. Zheng, X. Deng, State-of-health prediction for lithium-ion batteries with multiple Gaussian process regression model, IEEE Access 7 (2019) 150383–150394, http://dx.doi.org/10.1109/ACCESS.2019.2947294.